EXPERIMENTAL AND NUMERICAL STUDY OF ROTATING MAGNETIC FIELD DRIVEN FLOW IN CYLINDRICAL ENCLOSURES WITH DIFFERENT ASPECT RATIOS

Yu.M. Gelfgat[1] *, A.Yu. Gelfgat*[2]

[1] *Institute of Physics, University of Latvia, 32 Miera str., Salaspils, LV-2169, Latvia*
[2] *School of Mechanical Engineering, Faculty of Engineering, Tel-Aviv University, Ramat Aviv 69978, Israel*

Azimuthal velocities of the rotating magnetic field driven flow in a cylindrical container are measured in two different experiments for different aspect ratios (height/radius) of the container and different strengths of the magnetic field. The measured velocities are compared with the calculated ones. A good agreement between the experimental and numerical results is obtained. This validates the experimental techniques, the computational approach, and also the time-averaged model widely used in calculations of RMF-driven flows. It is shown that the average angular velocity normalized by the square root of the magnetic Taylor number grows linearly for the aspect ratios exceeding 1, and non-linearly for smaller aspect ratios. It is shown also that when the magnetic field is sufficiently large, the average angular velocity grows proportionally to the Hartmann number or proportionally to the square root of the magnetic Taylor number. It is shown that the dependence of the average angular velocity on the aspect ratio can be roughly approximated by a power of the ratio radius/height.

1. Introduction. Rotating magnetic fields (RMFs) are widely used in metallurgical and crystal growth technologies for controlling the melt flows and heat and mass transfer characteristics [1–3]. The rotating magnetic field induces a time-averaged azimuthal force, which drives the flow in circumferential direction. In its turn, non-uniform rotation of the liquid induces the azimuthal flow. All three components of the flow affect the heat and mass transfer processes thus yielding a powerful tool for flow and heat and mass transfer control. The RMF-driven flows have been intensively studied during two recent decades both experimentally and numerically (see [2–18] and references therein).

In spite of the large number of numerical studies of the RMF-induced flows, there are only few experimental investigations [2–9]. Most of experimental studies examine the influence of RMF on the temperature field or on the properties of grown crystals [2, 8–11], so avoiding the study of the flow field itself. There are very few attempts to measure the fluid velocities directly [3, 7, 14].

In the present study we report direct measurements of the azimuthal velocities of the RMF-driven flow in cylindrical containers of different aspect ratios (height/radius). The measured velocities are compared with the results of calculations, which, in their turn, are performed by two independent approaches. In this way we perform cross-validation of the experimental methodology with the calculations. The main set of results of the present study consists of the experimentally measured and numerically calculated dependencies of the azimuthal velocity in different radial and axial cross-sections of the container on the parameters of the RMF inductor and the geometry of the cylindrical container. A good agreement between the experimental and numerical results provides a rigorous experimental

validation of the widely used time-averaged RMF-driven flow model introduced in [12, 13].

2. Experimental technique and methodology. The experimental studies were performed by two different techniques. In the first series of experiments the azimuthal velocities were measured directly in different radial and axial cross-sections of the container for varying values of the magnetic field strength. In the second series the melt angular velocity was measured indirectly using the measurements of the pressure drop between the points located at the sidewall and at the center of the upper cover. The eutectic alloy InGaSn was used as a working liquid in both cases. The melting temperature of InGaSn is 10.5°C, and for temperature 20°C its electric conductivity is $\sigma = 3.3 \times 10^6$ $\Omega^{-1}\mathrm{m}^{-1}$, density $\rho = 6350$ $\mathrm{kg\,m^{-3}}$ and kinematic viscosity ν, according to different sources, varies from 3×10^{-7} to 3.5×10^{-7} $\mathrm{m^2s^{-1}}$.

In the first series of experiments the measurements were carried out in a cylindrical container made of acrylic plastic (Fig. 1). The inner diameter of the container was $D = 2R = 60$ mm. The height was varied by means of different cylindrical inserts, and in different experiments it was $H = 25, 30, 40, 50$ and 60 mm. In all experiments the container was completely filled with the alloy. To ensure wettability of the walls, the alloy was forcefully rubbed into the solid walls until a metallic film appeared on them.

The container with the alloy was axially aligned with the RMF inductor and positioned symmetrically with respect to its lower and upper ends. The RMF inductor was produced as an analog of the stator of a three-phase asynchronous electrical engine with the inner diameter of 213 mm and the height of the magnetic circuit of 100 mm (Fig. 1). The RMF inductor had 18 slots containing the coils with 130 windings each. The coils were connected into the two-pole circuits $(2p = 2)$ with two parallel branches. The maximal value of the magnetic field strength in the center of the inductor can reach 20 mT.

The RMF distribution in the working area of the inductor is given by a calibration curve, showing the dependence of the magnetic field strength B on the electric current I in the coils (Figs. 2 and 3). It is seen that in the area occupied
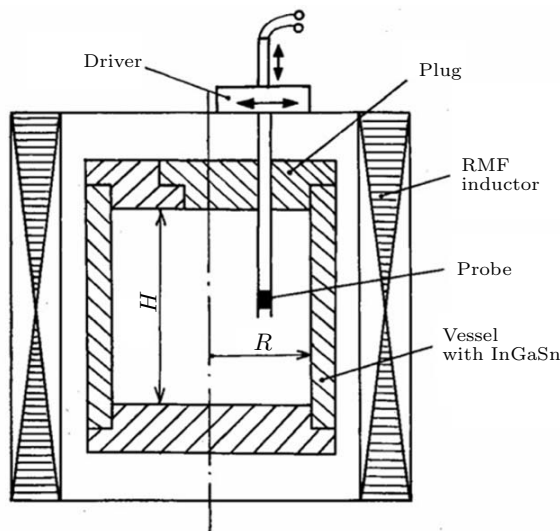

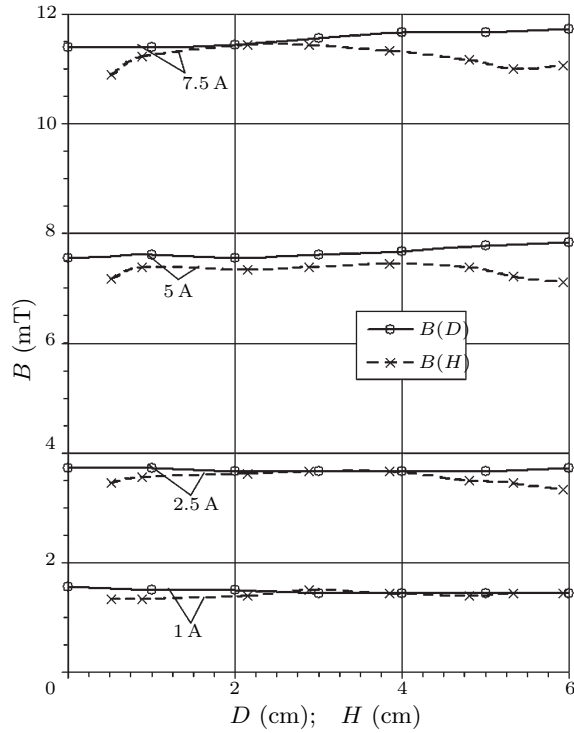*Fig. 1.* Sketch of the experimental setup used in the first series of experiments.

Fig. 2. Distribution of the magnetic field strength over the diameter $D = 2R$ and the height H at different values of the electric current in the inductor coils.

with the cylindrical container ($r \leq 30$ mm) the inhomogeneity of the magnetic field distribution does not exceed 0.5% for $B \leq 4$ mT, and 3% for $B \leq 7.5$ mT.

Velocity was measured by a special probe, which was constructed as a conductive anemometer with its own magnetic field [22, 23]. The conductive anemometer was made from a thin ceramic tube 3 mm indiameter. A longitudinally magnetized permanent magnet was mounted at one end of the tube. The diameter of the magnet is 2.5 mm and the magnetic field strength at its end is 0.3 T. The electrodes made from 0.1 mm diameter copper wire were mounted at the two opposite sides of the magnet and aligned along its axis. The electrodes ends protruded by 0.4 mm from the magnet end. Other ends of the electrodes passed through the
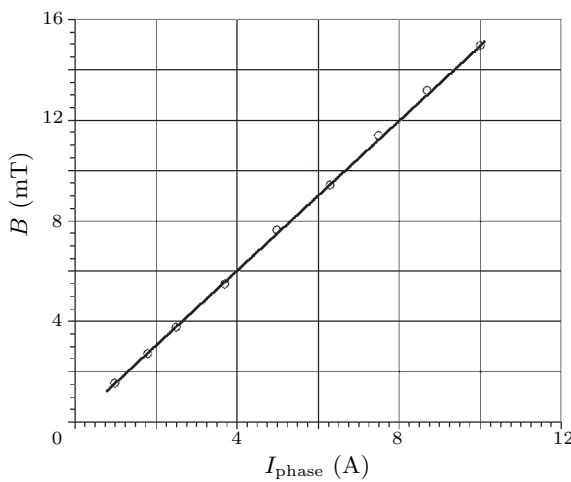

Fig. 3. Calibration curve of the RMF inductor in the center of the working volume.

ceramic tube and were attached to the terminal block. The whole probe, except the ends of the electrode near the magnet, was covered with lacquer insulation.

The probe was fixed in the holder of the traverse gear and could move along the radial 4 mm wide slot located in the upper cover of the container. After the probe was positioned at a necessary point, the slot was closed by a special plug, which was made flush-mounted with the container upper cover. The accuracy of the probe location in the radial and vertical directions was 0.1 mm. The voltage from the conductive anemometer was applied to a nano-voltmeter P341, from which it was transmitted to a programmable digital voltmeter B7-43. As a rule, each measurement was repeated not less than five times. Each of the five measurements was an average of 200 readings, which were registered by the voltmeter B7-43 at the same time intervals.

The probes were calibrated on a special calibration stand made as an annular duct filled with the InGaSn alloy and rotated mechanically with different angular velocities. Examples of the obtained calibration curves are shown in Fig. 4.

Measurements by the above described probes were possible for the container aspect ratios larger than $H/R \approx 0.8$. At smaller aspect ratios the probe-induced disturbances caused significant errors. Measurements for smaller aspect ratios called for another experimental approach, whose description follows. Three cylindrical cavities, made of acrylic plastic, with the inner diameter $D = 2R = 40$ mm and three different heights $H = 2, 5$ and 10 mm were used. Each cavity had two holes for pressure measuring, which were located at the center of the top cover and at the mid-height of its sidewall (Fig. 5). The holes were connected to a differential manometer consisting of a two-liquid (InGaSn and ethanol) hydraulic amplifier with an expanding tank and a tilted measuring U-tube [23]. The cavities were axially aligned inside the RMF inductor and arranged symmetrically with respect to its ends (Fig. 5). In this series of measurements we used a RMF inductor that had 4 poles with the coils on them. In this case, a symmetrically rotating magnetic field can be induced if the phase shift between the pairs of opposite coils
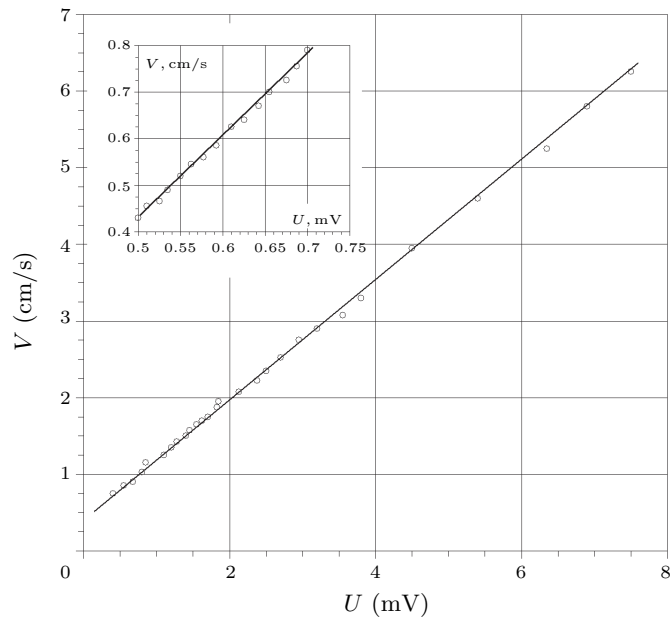

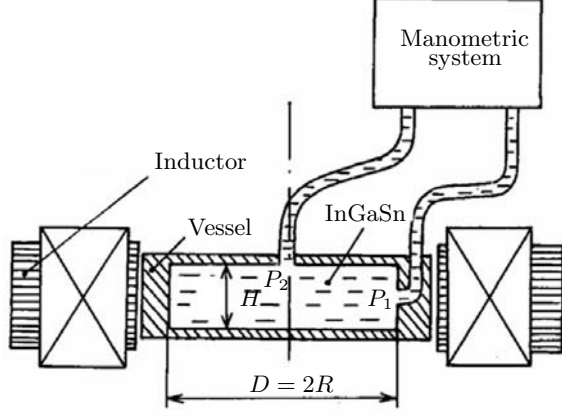*Fig. 4.* Calibration curve of the measuring probe.

Fig. 5. Sketch of the experimental setup used in the second series of experiments.

is 90°. The latter was achieved by a sequential connection of a capacitor in the circuit of one pair of the coils. The capacitance of the capacitor was calculated in advance. The electric currents in the circuits of each coil pairs were equalized by an adjustable resistor.

The magnetic field strength was varied by varying the voltage of the power supply. The calibration curves, showing the dependence of the magnetic field strength B on the electric current I in the coils, were obtained in the same way as in the first measurement series. The inhomogeneity of the magnetic field in the area occupied with a cavity did not exceed 3–4%.

The measurements were processed as follows. For each cavity the dependence of the pressure drop on the electric current $\Delta P = P_1 - P_2 = f(I)$ was measured. These dependences were recalculated into functions $v_\theta = f(B)$, where $v_\theta = \sqrt{2\Delta P/\rho}$ is the azimuthal velocity of the melt near the cavity sidewall, or into functions $\Omega = f(\mathrm{Ha})$, where Ω is the fluid angular velocity, and $\mathrm{Ha} = BR\sqrt{\sigma/\rho\nu}$ is the Hartmann number. Note that in both experimental series the actual value of the magnetic field B_{eff} differs from its amplitude value B_{A}, used in calculations, by the factor of $\sqrt{2}$, so that $B_{\mathrm{eff}} = B_{\mathrm{A}}\sqrt{2}$. Obviously, the value of the Hartmann number, used in the calculations below, must be changed by the same factor, i.e., $\mathrm{Ha}_{\mathrm{calc}} = \mathrm{Ha}_{\mathrm{exp}}\sqrt{2}$.

3. Formulation of the problem and numerical techniques. The mathematical problem was formulated on the basis of the model that accounts only for the time-averaged effect of the electromagnetic force induced by the rotating magnetic field. This model was introduced in [12, 13] and then was widely used in various numerical studies (see, for example, [14–18]). The fluid flow driven by the rotating magnetic field

$$\mathbf{B}_0(r, \theta, t) = B_0 \frac{r}{R_i} \left[\mathbf{e}_r \sin(p\theta - \omega t) + \mathbf{e}_\theta \cos(p\theta - \omega t) \right] \tag{1}$$

is described by the incompressible continuity and momentum equations

$$\nabla \cdot \mathbf{v} = 0, \tag{2}$$

$$\frac{\partial \mathbf{v}}{\partial t} + (\mathbf{v} \cdot \nabla)\mathbf{v} = -\nabla p + \Delta \mathbf{v} + \mathrm{Ta}_{\mathrm{m}} \left[-\nabla(\phi_1 + \phi_2) + r\mathbf{e}_\theta \right] \tag{3}$$

where (r, θ, z) are the cylindrical coordinates, R_i is the radius of a RMF inductor, ω is the circular frequency of magnetic field rotation, $\mathbf{v} = \{u_r, u_\theta, u_z\}$ and p are

151

the fluid velocity and pressure, respectively, and ϕ_1 and ϕ_2 are parts of the electric potential of the RMF-induced currents. The scales of length, time, velocity and pressure used to render Eqs. (1)–(3) dimensionless are R, R^2/ν, ν/R, and $\rho\nu^2/R^2$, respectively. With these scales the RMF forcing is defined by the rotating magnetic field Taylor number $\mathrm{Ta_m} = B_0^2 R^4 \sigma\omega/2\rho\nu^2$. The parts of the electric potential ϕ_1 and ϕ_2 are defined by the following problems

$$\Delta\phi_1 = \frac{1}{\mathrm{Re}_\omega}\left(\frac{1}{r}\frac{\partial u_r}{\partial\varphi} - \frac{\partial u_\varphi}{\partial z}\right), \qquad \left.\frac{\partial\varphi_1}{\partial n}\right|_\Gamma = \left(\mathbf{e}_z \cdot \frac{\mathbf{n}}{|\mathbf{n}|}\right)r. \tag{4}$$

$$\Delta\phi_2 = \frac{1}{\mathrm{Re}_\omega}\left(\frac{\partial u_r}{\partial z} - \frac{\partial u_z}{\partial r}\right), \qquad \left.\frac{\partial\varphi_2}{\partial n}\right|_\Gamma = 0. \tag{5}$$

Here $\mathrm{Re}_\omega = \omega R^2/\nu$ is the rotating magnetic field Reynolds number. The three governing parameters Ha, $\mathrm{Ta_m}$ and Re_ω are related as:

$$\mathrm{Ta_m} = \frac{1}{2}\mathrm{Ha}^2\mathrm{Re}_\omega, \tag{6}$$

so that only two of them are independent. We have found that sometimes it is more convenient to use the Hartmann number instead of the Taylor number.

The RMF Reynolds number Re_ω is usually very large and in most numerical works the right-hand side (r.h.s.) of Eqs. (4) and (5) is neglected. In this case, $\phi_2 = 0$ and the problem (4), (5) for ϕ_1 allows for an analytical solution [25]. We, however, prefer not to neglect the effect of Re_ω and solve the problems (4), (5) and (6), (7) numerically. Our computational experiments show that the r.h.s. of (4) indeed can be neglected for $\mathrm{Re}_\omega > 10^5$, which is consistent with the similar conclusion made in [14].

The calculations were carried out using two independent numerical approaches, which cross-validated each other. The first approach is based on the global Galerkin method [19] and calculates the steady solution directly by the Newton method. The second one is based on the finite volume discretization in space and applies the SIMPLE time-integration scheme to reach the steady-state solution. This approach has been successfully used for calculating the rotating flows in a cylinder [20] and is applied here for validation purposes only. The calculations performed by the global Galerkin method used from 20 to 60 basis functions in each spatial direction, depending on the values of the aspect ratio and the RMF Taylor number. The calculations by the finite volume method were done using stretched staggered grids with the number of nodes varying from 50 to 200 in each spatial direction. The results obtained by the both numerical methods differed in less than 1%. The difference in the results is caused mainly by the discontinuity in the boundary condition for the electric potential (5). This discontinuity is treated differently by the two methods that leads to certain, however, negligible discrepancies.

To compare with the experimental results, it is necessary to remove the uncertainty in the kinematic viscosity value of the InGaSn alloy. Upon completion of the first series of calculations, it has been found that the best agreement with the experimental and numerical results is reached for $\nu = 3.03 \times 10^{-7}$ m^{2}s^{-1}, which falls within the range of the values reported in literature. This yields for the first series of the experiments described above: $\mathrm{Re}_\omega = 9.33 \times 10^5$, $\mathrm{Ha} = 1.24 \times 10^3 B$, $\mathrm{Ta_m} = 7.20 \times 10^{11}B^2$, and for the second series: $\mathrm{Re}_\omega = 4.15 \times 10^5$, $\mathrm{Ha} = 0.83 \times 10^3 B$, $\mathrm{Ta_m} = 1.42 \times 10^{11}B^2$. Here B is the amplitude value of the magnetic field measured in Teslas.

It is emphasized that in the following we consider only steady states of the RMF-driven flows regardless of their possible instability [17,18] or multiplicity

152

[21]. We are aware of the fact that according to the results of [17,18] the flow becomes unstable at $Ta_m > 10^5$. We tried to reproduce these results using the global Galerkin method [19], which is developed for such kind of stability studies. However, we have failed to reach the convergence in the critical RMF Taylor number. A good agreement between the experimental measurements and the steady state calculations, obtained up to $Ta_m > 6 \times 10^6$, shows that the instability, if exists, does not change the flow pattern significantly.

4. Results. The measurements performed for different values of the aspect ratio and the Hartmann (or RMF Taylor) number were compared with the numerical results. Only steady flows regardless of their stability were calculated in the numerical study. A characteristic example is given in Figs. 6–8 for the series of experiments in the container with the aspect ration $H/R = 2$. On these graphs the experimental and numerical results are shown as points and solid lines, respectively. Fig. 6 illustrates the dependence of the azimuthal velocity at point $r = R/2$, $z = H/2$ at different RMF Taylor numbers (i.e., different values of the magnetic field strength). Velocity profiles at different radial and axial cross-sections are shown in Figs. 7 and 8, respectively.

Comparison of the experimental and numerical results (Figs. 6–8) shows a good agreement everywhere except the points located near the cylinder sidewall. There the accuracy of the experimental measurements by the above described probe is significantly lower, so that the deviation between the numerical and the experimental results exceeds 10% .

Fig. 6 shows the dependence of the azimuthal velocity at point $r = R/2$, $z = H/2$ on the RMF Taylor number for the cylinder with the aspect ratio $H/R = 2$. It is seen that the measured values perfectly fit the numerical curve. Note that according to the numerical results of [17, 18], the flow is unstable beyond $Ta_m > 10^5$. Thus, the deviation of the experimentally measured time-averaged velocity from the result of the steady-state calculation can be expected at larger Ta_m, when pulsating components gather significant part of the flow energy. However, no deviation is observed. This means, assuming that the instability was detected
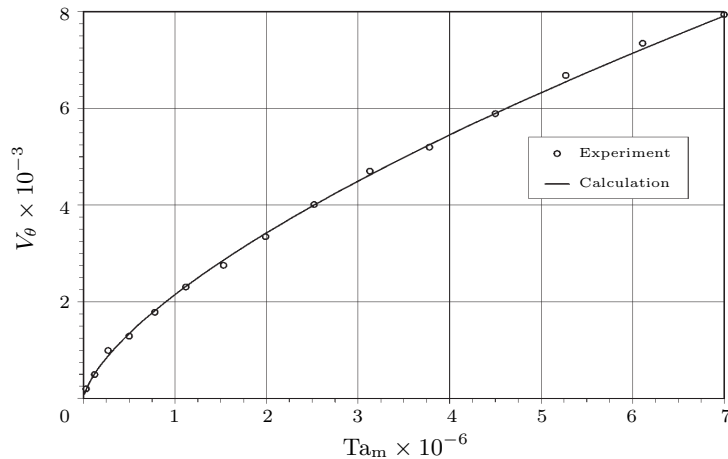

Fig. 6. Dependence of the dimensionless azimuthal velocity on the RMF Taylor number at point $r = R/2$, $z = H/2$. Calculation and measurements for $H/R = 2$, $B = 2.1$ mT, $Ta_m = 3.03 \times 10^6$, Ha = 2.58.
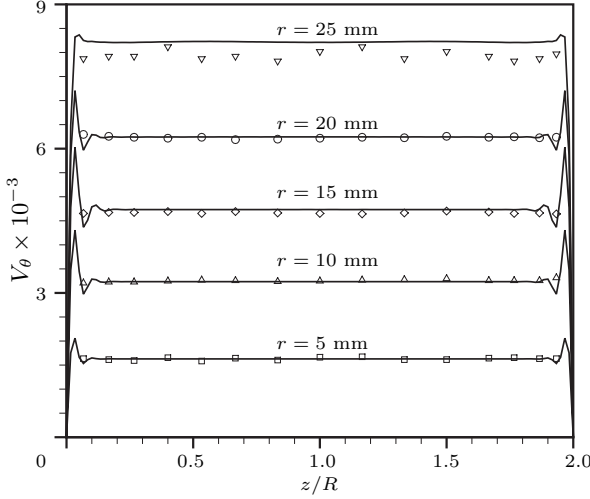
Fig. 7. Azimuthal velocity profiles in different radial cross-sections. Calculation and measurements for $H/R = 2$, $B = 2.1$ mT, $\mathrm{Ta_m} = 3.03 \times 10^6$, $\mathrm{Ha} = 2.58$.

correctly, that the azimuthal component of the flow is not noticeably affected by the instability. A larger effect can be possibly observed in the meridional flow.

Fig. 7 shows some profiles of the azimuthal velocity in different radial cross-sections of the meridional plane. As mentioned, the agreement between calculation and measurement is observed everywhere except the cross-section $r = 25$ mm, which is located close to the cylinder sidewall. As mentioned above, precise measurements are impossible in the region.

The azimuthal velocity profiles in the axial cross-sections are shown in Fig. 8. Note that the shape of the profiles is almost independent on the axial coordinate. As above, the disagreement between experiment and calculation is observed only close to the cylinder sidewall (i.e., $r = R$).

Fig. 9 compares the measured and the calculated averaged angular velocity for different aspect ratios and different values of the RMF Taylor (or Hartmann) number. For all values of the aspect ratio, $H/R = 0.833$, 1.333, 1.667 and 2, there is a good agreement between the experimental and numerical results. Growth of the aspect ratio reduces the effect of friction at the top and at the bottom. As a result, the average rotation grows with the increase of H/R.

The measurements in the second series of experiments were possible only at relatively large values of the Hartmann number, $\mathrm{Ha} > 8$, which implies $\mathrm{Ta_m} > 7.5 \times 10^6$. This restriction is caused by the accuracy of the pressure drop measurements by the above manometer system. The obtained results, showing the dependence of the averaged angular velocity on the RMF Taylor number for $H/R = 0.1$, 0.25 and 0.5, are shown in Fig. 10. As expected, with the decrease of the aspect ratio H/R the angular velocity decreases. This leads to further measurement restrictions, so that at $H/R = 0.1$ reliable results could be obtained only for $\mathrm{Ha} > 20$.

The comparison of all experimental and numerical results for all values of the aspect ratios considered is illustrated in Fig. 11 as a dependence of the averaged angular velocity on the aspect ratio. The angular velocity is scaled by $\sqrt{2\mathrm{Ta_m}} = \mathrm{Ha}\sqrt{\mathrm{Re_\omega}}$. As seen from the figure, the results agree better for larger values of the aspect ratio. It should be emphasized that starting from $H/R = 1$ and for larger aspect ratios the dependence of the angular velocity on the Hartmann number is linear, assuming that the RMF Reynolds number is constant. Consequently, this dependence behaves as $\sqrt{\mathrm{Ta_m}}$ for large aspect ratios.

From the practical point of view it would be interesting to estimate how the average angular velocity varies with the variation of the container aspect ratio and
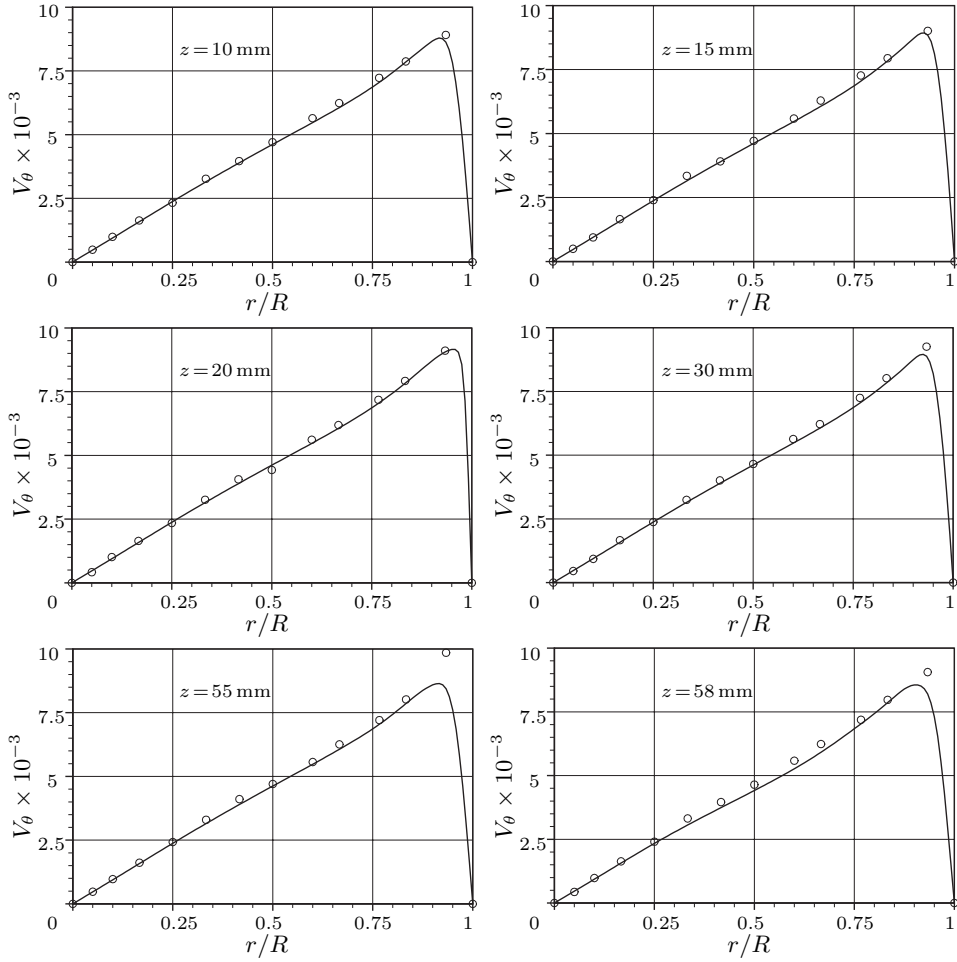
154

Fig. 8. Azimuthal velocity profiles in different axial cross-sections. Calculation and measurements for $H/R = 2$, $B = 2.13$ mT, $Ta_m = 3.12 \times 10^6$, $Ha = 2.62$.
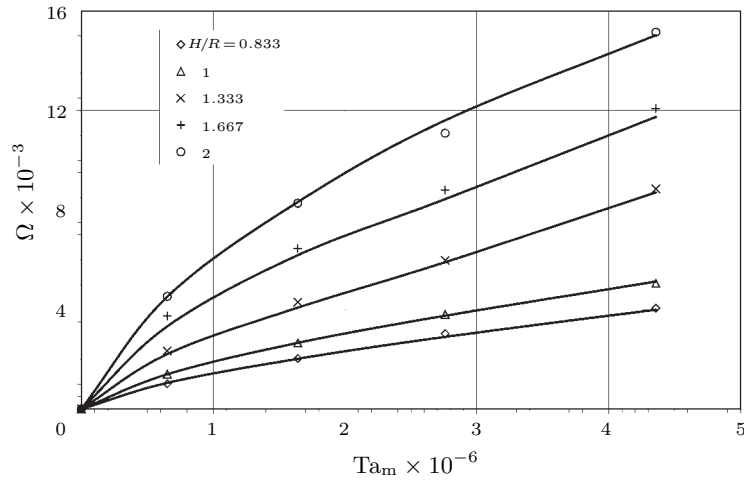

Fig. 9. Dependence of the average angular velocity on the Hartmann number for different aspect ratios. Measurements of the first series of experiments, $0 < Ha < 3.5$.
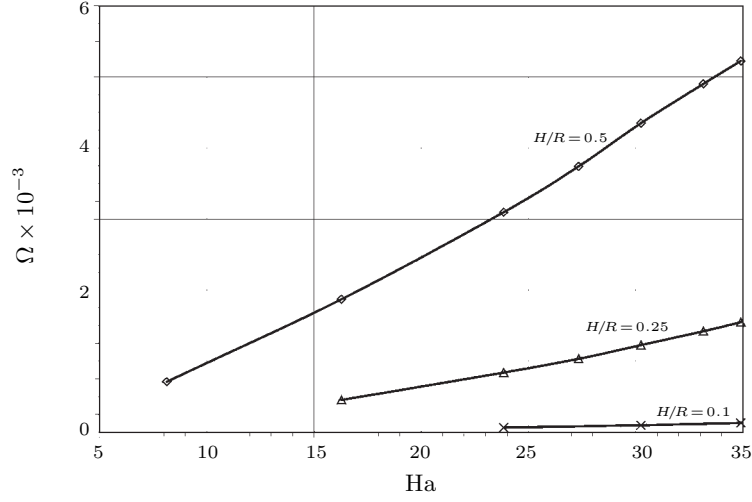
Fig. 10. Dependence of the averaged angular velocity on the Hartmann number for different aspect ratios. Measurements of the second series of experiments, $5 < \text{Ha} < 35$.

the magnetic field. Such an attempt is made in Fig. 12, where we use the data of two experiments reported here and the results of another experiment [7]. Note that the average angular velocity in Fig. 12 is dimensional (rad/s). It happens that the linear dependence on the Hartmann number can be found if the average angular velocity is scaled by $(H/R)^{1.8}$ for small aspect ratios ($H/R < 0.5$, Fig. 12*a*), by $(H/R)^{1.5}$ for the aspect ratios close to unity ($0.8 < H/R < 2$, Fig. 12*b*) and by R/H for large aspect ratios ($H/R > 2$, Fig. 12*c*). These scalings yield for large Hartmann numbers:

$$\Omega \approx -7.6 + 0.65 \text{Ha} \left(\frac{H}{R}\right)^{1.8} \quad \text{for } H/R < 0.5; \tag{7}$$

$$\Omega \approx -0.96 + 1.6 \text{Ha} \left(\frac{H}{R}\right)^{1.5} \quad \text{for } 0.8 < H/R < 2; \tag{8}$$
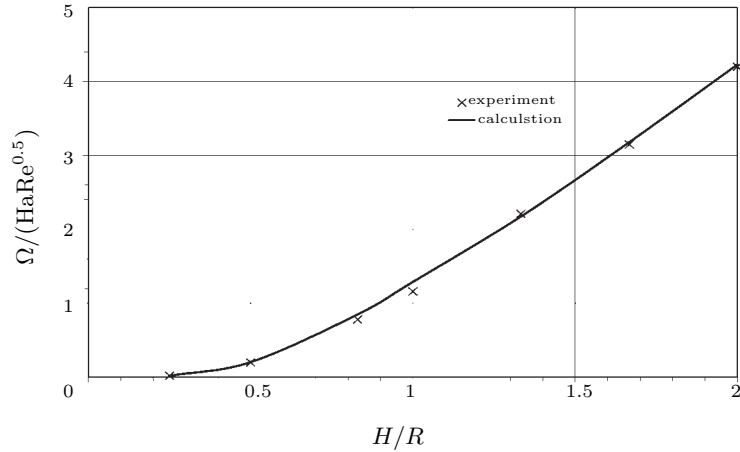

Fig. 11. Comparison of the measured and calculated values of the averaged angular velocity.
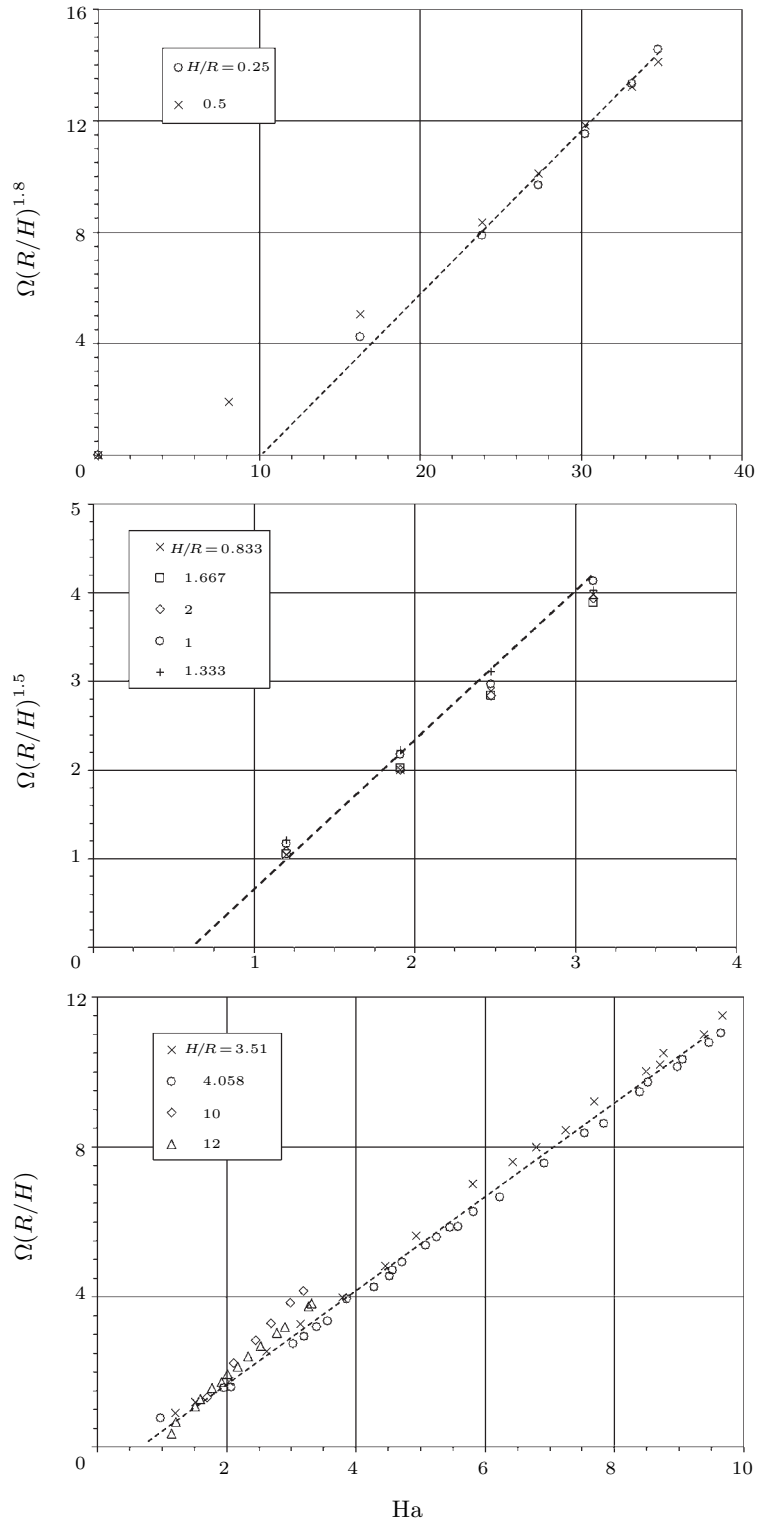
156

Fig. 12. Scaling of the average angular velocity by the aspect ratio and the Hartmann number for (*a*) $H/R \leq 0.5$, (*b*) $0.8 \leq H/R \leq 2$, (*c*) $H/R > 3$ (data is taken from [7]).

$$\Omega \approx -0.75 + 1.25 \text{Ha} \frac{H}{R} \quad \text{for } H/R > 2. \tag{9}$$

Hence, it is expected that at large Ha the average angular velocity varies as $\text{Ha}(H/R)^{\alpha}$, where α also depends on the aspect ratio, but varies slowly from $\alpha \approx 2$ at small H/R to $\alpha \approx 1$ at large H/R.

5. Conclusions. The experimental and numerical results reported here yield a quantitative validation of the RMF driving force time-averaged model formulated in [12, 13] and widely used in various studies (e.g., [12–18]).

Obviously, the rotating magnetic field induces a rather intensive rotating motion in a cylindrical container filled with an electrically conducting fluid. The reported experimental results show that with the increase of the relative height of the cylindrical container the average rotation of the fluid increases faster at lower aspect ratios of the cylindrical container ($H/R < 1$). Beyond the value of $H/R = 1$ the growth is linear. Moreover, at large aspect ratios, i.e., $H/R > 1$, the dependence of the averaged rotation on the Hartmann number is linear that implies that the average rotation at the fixed RMF Reynolds number grows as $\sqrt{\text{Ta}_{\text{m}}}$. The dependence of average rotation on the aspect ratio of the container is more complicated. It is shown that at large Hartmann numbers this dependence can be roughly estimated as $(R/H)^{\alpha}$, where power α varies from $\alpha \approx 2$, characteristic for very low cylinders, to $\alpha \approx 1$ for high cylinders.

REFERENCES

[1] J.P. BIRAT, J. CHONE. Electromagnetic stirring on billet, bloom and slab continuous casters: state of art in 1982. *Ironmaking and Steelmaking*, vol. 10 (1983), pp. 269–281.

[2] YU.M. GELFGAT, J. PRIEDE. MHD flow in a rotating magnetic field (review). *Magnetohydrodynamics*, vol. 32 (1995), no. 2, pp. 188–200.

[3] P. DOLD, K.W. BENZ. Rotating magnetic field: fluid flow and crystal growth applications. Progress in Crystal Growth and Characterization of Materials. *An International Review Journal*, vol. 38 (1999), no. I-4, pp. 7–38.

[4] B.I. DORONIN, V.V. DREMOV, A.B. KAPUSTA. Measurement of the MHD mercury flow characteristics in a closed cylindrical container. *Magnetohydrodynamics*, vol. 9 (1973), no. 3, pp. 412–413.

[5] V.P. SHAMOTA. Rotation of a conducting fluid by an electromagnetic field. *Magnetohydrodynamics*, vol. 33 (1997), no. 1, pp. 34–37.

[6] A.B. KAPUSTA, A.F. ZIBOLT. Three-dimensional effects in a container of finite length in a rotating magnetic field. *Magnetohydrodynamics*, vol. 18 (1982), no. 4, pp. 379–382.

[7] A.B. Kapusta, V.P. Shamota. Turbulent rotating MHD flow in finite length cylindrical container. In: *Proc. 4th Int. Conf. on Magnetohydrodynamic at Dawn of Third Millennium* (Presqu'ile de Giens, France, September 18-22, 2000), pp. 681–686.

[8] A. Cröll, P. Dold, Th. Kaiser, F.R. Szofran, K.W. Benz. The influence of static and rotating magnetic fields on heat and mass transfer in silicon floating zones. *J. Electrochem. Soc.*, vol. 146 (1999), pp. 2270–2275.

[9] B. Fischer, J. Friedrich, H. Weimann, G. Müller. The use of time-dependent magnetic fields for control of convective flows in melt growth configurations. *J. Crystal Growth*, vol. 198/199 (1999), pp. 170–175.

[10] M.P. Volz, K. Mazuruk. An experimental study of the influence of a rotating magnetic field on Rayleigh–Benard convection. *J. Fluid Mech.*, vol. 444 (2001), pp. 79–98.

[11] I. Grants, G. Gerbeth. Experimental study of non-normal nonlinear transition to turbulence in a rotating magnetic field driven flow. *Phys. Fluids*, vol. 15 (2003), pp. 2803–2809.

[12] J. Priede. *Theoretical study of a flow in an axisymmetric cavity of finite length, driven by a rotating magnetic field* (PhD Thesis, Salaspils, Latvia, 1993).

[13] Yu.M. Gelfgat, J. Priede, M.Z. Sorkin. Numerical simulation of MHD flow induced by a magnetic field in a cylindrical container of finite length. *Proc. Int. Conf. on Energy Transfer in MHD Flows* (Grenoble, France, 1991), pp. 181–186.

[14] R.U. Barz, G. Gerbeth, U. Wunderwald, E. Buhrig, Yu.M. Gelfgat. Modeling of the isothermal melt flow due to rotating magnetic field in crystal growth. *J. Crystal Growth*, vol. 180 (1997), pp. 410–421.

[15] L. Martin Witkowsky, P. Marty. Effect of a rotating magnetic field of arbitrary frequency on a liquid metal column. *Eur. J. Mech., B/Fluids*, vol. 17 (1998), pp. 239–254.

[16] D. Vizman, B. Fischer, J. Friedrich, G. Müller. 3D numerical simulation of melt flow in the presence of a rotating magnetic field. *Int. J. Numer. Meth. Heat Fluid Flow*, vol. 10 (2000), pp. 366–384.

[17] I. Grants, G. Gerbeth. Stability of axially symmetric flow driven by a rotating magnetic field in a cylindrical cavity. *J. Fluid Mech.*, vol. 431 (2001), pp. 407–426.

[18] I. Grants, G. Gerbeth. Linear three-dimensional instability of magnetically driven rotating flow. *J. Fluid Mech.*, vol. 463 (2002), pp. 229–239.

[19] A.Yu. Gelfgat. Two- and three-dimensional instabilities of confined flows: numerical study by a global Galerkin method. *Computational Fluid Dynamics Journal*, vol. 9 (2001), pp. 437–448.

[20] A.Yu. Gelfgat, P.Z. Bar-Yoseph, A. Solan. Stability of confined swirling flow with and without vortex breakdown. *Journal of Fluid Mechanics*, vol. 311 (1996), pp. 1–36.

[21] A. Yu. Gelfgat, P.Z. Bar-Yoseph. Multiple solutions and stability of confined convective and swirling flows – a continuing challenge. *Int. J. Numer. Meth. Heat and Fluid Flow*, vol. 14, pp. 213–241.

[22] V.T. Weisenfluh. Probes for local velocity and temperature measurements in liquid metal flow. *International Journal of Heat and Mass Transfer*, vol. 28 (1985), no. 8, pp. 1563–1574.

[23] R. Ricon, C. Vices. Local velocity and mass transfer measurement in molten metals using on incorporated magnetic probe. *International Journal of Heat and Mass Transfer*, vol. 25 (1982), pp. 1579–1588.

[24] H. Branover. *Turbulent MHD flows in pipes* (Zinatne Publishing House, Riga, 1967), 131 p. (in Russian).

[25] L.P. Gorbachev, N.V. Nikitin, A.L. Ustinov. Magnetohydrodynamic rotation of an electrically conductive liquid in a cylindrical container of finite dimensions. *Magnetohydrodynamics*, vol. 10, no. 4 (1974), pp. 406–414.